LEGIBILITY NOTICE

A major purpose of the Technical Information Center is to provide the broadest dissemination possible of information contained in DOE's Research and Development Reports to business, industry, the academic community, and federal, state and local governments.

Although a small portion of this report is not reproducible, it is being made available to expedite the availability of information on the research discussed herein.

LA-UR -89-1230

Los Alamos National Laboratory is operated by the University of California for the United States Department of Energy under contract W-7405-ENG-36

DE89 011185

LA-UR--89-1230

TITLE **CHERENKOV WAKEFIELD ACCELERATORS: RIPPLED WAVEGUIDES**

AUTHOR(S) **Michael E. Jones, R. K. Keinigs, W. Peter and S. C. Wilks**

SUBMITTED TO **Proceedings of the 1989 Workshop on Advanced Accelerator Concepts**

DISCLAIMER

Los Alamos National Laboratory
Los Alamos, New Mexico 87545

CHERENKOV WAKEFIELD ACCELERATORS: RIPPLED WAVEGUIDES*.

Michael E. Jones, R. K. Keinigs, W. Peter and S. C. Wilks†
Los Alamos National Laboratory, Los Alamos, NM 87545

ABSTRACT

The properties of using periodically rippled waveguides as wakefield accelerators are invesitgated. An analysis is performed in the ultrarelativistic limit which accurately predicts the amplitude, wavelength of the wakefield, and their dependences on waveguide and drive beam parameters. These devices are found to have the properties that the synchronous transverse wake vanishes, and the accelerating field is independent of the radial position in the drift tube and independent of the radial profile of the drive beam current. The effects of the nonsynchronous wakefields are discussed. Also, particle-in-cell simulations are performed which agree with the analysis and reveal self-consistent and collective effects in particle acceleration.

INTRODUCTION

One of the most promising new concepts for future high gradient relativistic electron accelerators is the wakefield accelerator idea. Wakefield accelerator concepts have several advantages over conventional accelerators. Because the the beam to be accelerated follows immediately behind the driving beam the accelerating field produced by the driving beam has much less time to cause breakdown of the structure. Furthermore, in principle, the efficiency with which energy is extracted from the drive beam can be made arbitrarily high with proper shaping of the beam.

Although the properties of wakefields and their possible use for acceleration had been known for some time, the idea of a wakefield accelerator gained popularity with the radial wakefield transformer proposed by Voss and Weiland.[1] Because of the high limiting electric fields obtainable in plasmas and the relative simplicity of plasma waves, the concept of the plasma wakefield accelerator (PWA) was proposed[2,3] and subsequently received the most attention. The plasma accelerators really exhibit advantages over other concepts only at frequencies greater than about 100 Ghz.[4] Unfortunately, the problem of producing a suitable drive beam becomes more difficult as the frequency is increased. Furthermore, because the drive beam is space-charge neutralized by the plasma, but not completely current neutralized, it is difficult to maintain the drive beam pulse shape because of the transverse wake that is generated even for azimuthally symmetric drive beams.[5] Possible solutions to the latter problem have been studied[6]. However, if one is willing to consider more modest accelerating gradients (a few hundred MV/m), a class of wakefield accelerators we call Cherenkov wakefield accelerators are worth considering.

Cherenkov wakefield accelerators (CWA) use electromagnetic waves generated by a beam traveling through a slow-wave structure to accelerate a trailing bunch. Because the

* This work was performed under the auspices of the U.S. Dept. of Energy

† Permanent Address: University of California at Los Angeles, Los Angeles, Ca.

beams propagate in vacuum in these devices the transverse wake moving synchronously with an azimuthially symmetric drive beam will cancel to $1/\gamma^2$, where γ is the relativistic factor for the drive beam. Actually all wakefield field accelerators, other than the PWA which uses electrostatic waves, can be classed as CWAs. However, we have in mind particularly simple devices such as dielectrically filled waveguides and waveguides with periodically varying walls. Other structures with similar properties include ferrite lined waveguides[7] and periodic cavity structures.[8]

Recent work on dielectric structures have shown that wakefields can be excited in these devices and they have the potential for being used as accelerators.[9,10] However, there are uncertainties about the limits and effects of dielectric breakdown at high frequency, high field conditions. In this paper we consider a CWA which uses a rippled waveguide as the slow wave structure. This device is expected to have better breakdown tolerances than structures involving dielectrics or ferrites. Furthermore, because the wall is smoothly varying, there will not be the large field enhancements found at the edges of the holes in periodic cavity structures.

The paper is organized as follows. A simple analysis of the wakefield in a rippled waveguide is given in the next section and scaling laws are discussed for wakefield acceleration. The following section describes the numerical model used to simulate these devices, including self-consistent dynamics of the driving and accelerated beams. Finally a description of the particle-in-cell simulations of representative cases is given.

ANALYSIS OF RIPPLED WAVEGUIDES

Analytic calculations of wakefields in periodic waveguides have been performed previously by several researchers.[11-13] In this section we calculate the wakefield for the specific case of a sinusoidally rippled waveguide and discuss the implications for wakefield accelerators. Our analysis is essentially a simplified and specialized version of the work by Cooper, Krinsky and Morton.[12]

We wish to find the wakefield in a long drift tube or waveguide whose wall radius r_w varies periodically with axial position, z as

$$r_w = a[1 + \epsilon s(z)] \tag{1}$$

where a is the mean radius of the guide and $s(z) = \cos(k_0 z)$. The parameter ϵ is the ratio of the ripple depth to the mean guide radius and will be assumed to be much less than unity for the purposes of the analysis.

To calculate the wakefield, we solve Maxwell's equations in an axisymmetric system for the electric field components E_z and E_r and magnetic field component B_θ for a specified drive beam source subject to the boundary condition that the tangential electric field vanish along the waveguide wall. This boundary condition can be expressed as

$$E_z = -\epsilon a \frac{ds}{dz} E_r \tag{2}$$

where Eq. (2) is evaluated at the radial position given by Eq. (1). For $\epsilon \ll 1$ this boundary condition can be approximated by expanding Eq. (2) in a power series in ϵ about the mean guide radius, a to obtain

$$E_z(a) \approx -\epsilon a\left(s' E_r(a) + s\frac{\partial E_z(a)}{\partial r}\right) - \frac{\epsilon^2 a^2}{2}\left(2ss'\frac{\partial E_r(a)}{\partial r} + s\frac{\partial^2 E_z(a)}{\partial r^2}\right) + \ldots \tag{3}$$

where the prime denotes differentiation with respect to z. Furthermore the electric fields can be expanded in powers of ϵ so that

$$\mathbf{E} = \mathbf{E}^{(0)} + \epsilon\mathbf{E}^{(1)} + \epsilon^2\mathbf{E}^{(2)} + \ldots \tag{4}$$

Using Eq. (4) in Eq. (3), one obtains to second order in ϵ

$$\begin{aligned} E_z^{(0)}(a) &= 0; \\ E_z^{(1)}(a) &= -a[s' E_r^{(0)}(a) + s\partial E_z^{(0)}(a)/\partial r]; \\ E_z^{(2)}(a) &= -a[s' E_r^{(1)}(a) + s\partial E_z^{(1)}(a)/\partial r] \\ &\quad - a^2 s[s'\partial E_r^{(0)}(a)/\partial r + (s/2)\partial^2 E_z^{(0)}(a)/\partial r^2] \end{aligned} \tag{5}$$

In the ultrarelativistic approximation, the lowest order solution for an infinitesimally thin beam on axis with total current $I(ct - z)$ is

$$\begin{aligned} E_z^{(0)} &= 0, \\ E_r^{(0)} &= B_\theta^{(0)} = 2I(ct - z)/rc. \end{aligned} \tag{6}$$

Using this expression in Eq. (5), the boundary condition for the first order axial electric field becomes

$$E_z^{(1)}(a) = -2s' I(ct - z)/c. \tag{7}$$

Defining the double Fourier transform in t and z as

$$\hat{E}(r, k, \omega) \equiv \frac{1}{(2\pi)^2}\int_{-\infty}^{+\infty} dt \int_{-\infty}^{+\infty} dz e^{-i(kz - \omega t)} E(r, z, t) \tag{8}$$

one obtains from Maxwell's equations for a thin beam

$$\frac{1}{r}\frac{\partial}{\partial r}\left(r\frac{\partial \hat{E}_z}{\partial r}\right) + \left(\frac{\omega^2}{c^2} - k^2\right)\hat{E}_z = -2i\hat{I}(k)\frac{\delta(r)}{r}\frac{(\omega^2 - k^2c^2)}{\omega c}\delta(\omega - kc). \tag{9}$$

Because of the $\delta(\omega - kc)$ in the source term we get no contribution from the right hand side when we invert the transform. Therefore we only need to solve the homogeneous form of Eq. (9). The solution to the homogeneous equation can be written as

$$\tilde{E}_z(r,k,\omega) = \tilde{E}_z(a,k,\omega)\frac{J_0(\kappa r)}{J_0(\kappa a)}, \tag{10}$$

where $\kappa^2 \equiv \omega^2/c^2 - k^2$ and J_0 is the Bessel function of zero order.

Because of the linearity of Maxwell's equations, Eq. (10) is valid to all orders in ϵ. To apply it we must Fourier transform Eq. (7) using Eq. (8). For a uniform bunch with current I_0 and vanishing length L, such that the total charge $Q = I_0 L/c$ remains finite, this procedure gives

$$\tilde{E}_z^{(1)}(a,k,\omega) = Q\frac{ik_0}{2\pi}\{\delta[(k+k_0)c-\omega] - \delta[(k-k_0)c-\omega]\}. \tag{11}$$

We can use this expression in Eq. (10) and invert the Fourier transforms to get the axial field behind the driving bunch to first order in ϵ:

$$E_z(r,z,t) \approx \frac{2Q\epsilon}{a^2}\sum_{n=1}^{\infty} p_n \frac{J_0(p_n r/a)}{J_1(p_n)} cos[k_n z - (k_n - k_0)ct] \tag{12}$$

where $k_n \equiv (k_0/2)[1 - p_n^2/(k_0 a)^2]$ and p_n is the nth zero of $J_0(x)$. None of the modes have a phase velocity equal to c. This means that the first order wakefield is nonsynchronous with an ultrarelativistic particle. The synchronous or accelerating fields appear only in second order in ϵ.

Fourier transforming the last equation in Eq. (5) we obtain

$$\begin{aligned}\tilde{E}_z^{(2)}(a,k,\omega) = -\frac{a}{2}\Bigg[&\left(\frac{k_0(k+k_0)}{\omega^2/c^2-(k+k_0)^2}+1\right)\frac{\partial\tilde{E}_z^{(1)}}{\partial r}(a,k+k_0,\omega)\\ &-\left(\frac{k_0(k-k_0)}{\omega^2/c^2-(k-k_0)^2}-1\right)\frac{\partial\tilde{E}_z^{(1)}}{\partial r}(a,k-k_0,\omega)\Bigg]\\ &+Q\frac{ik_0}{4\pi}\{\delta[(k+2k_0)c-\omega]-\delta[(k-2k_0)c-\omega]\}\end{aligned} \tag{13}$$

where we have used

$$\tilde{E}_r(r,k,\omega) = \frac{ik}{\omega^2/c^2-k^2}\frac{\partial\tilde{E}_z}{\partial r}(r,k,\omega). \tag{14}$$

From Eq. (10) we obtain

$$\frac{\partial\tilde{E}_z^{(1)}}{\partial r}(a,k,\omega) = -\kappa\tilde{E}_z^{(1)}(a,k,\omega)\frac{J_1(\kappa a)}{J_0(\kappa a)} \tag{15}$$

Because of the delta functions in Eq. (11), when it is used in Eq. (15) and the result is used in Eq. (13), there will be synchronous terms to second order in ϵ, i.e. terms involving $\delta(kc-\omega)$. Furthermore, when these terms are used in Eq. (10), the delta function will set

$\kappa = 0$, so that we find E_z for the synchronous modes will be independent of r. Thus we obtain

$$\begin{aligned}\tilde{E}_z^{(2)}(r,k,\omega) &= \tilde{E}_z^{(2)}(a,k,\omega) \\ &= \frac{iQkk_0^2a}{4\pi}\left[\frac{J_1(\kappa_+a)}{\kappa_+J_0(\kappa_+a)} + \frac{J_1(\kappa_-a)}{\kappa_-J_0(\kappa_-a)}\right]\delta(kc-\omega) \\ &+ \text{nonsynchronous terms} \end{aligned} \tag{16}$$

where $\kappa_\pm \equiv -k_0(k_0 \pm 2k)$. Keeping only the synchronous terms we find after inverting the Fourier transforms

$$E_z(r,z,t) \approx Qk_0\epsilon^2 \sum_{m=1}^{\infty} k_m \cos[k_m(z-ct)] \tag{17}$$

where $k_m \equiv (k_0/2)[1 + p_m^2/(k_0a)^2]$. Note the difference in sign from the definition of k_n in Eq. (12). Furthermore, the transverse wakeforce $E_r - B_\theta$ is zero for the synchronous fields, because the E_r and B_θ fields which vary linearly with r cancel exactly in the ultrarelativistic limit assumed in this analysis.

A point particle moving through the rippled waveguide will excite the fields given by Eq. (12), which are first order in ϵ. These fields are thus larger than the synchronous fields given by Eq. (17) which are second order in ϵ. However, because they are nonsynchronous, the first order fields alternately take energy from and give energy back to the particle and the fields given by Eq. (17) are the lowest order approximation to the fields which can extract energy from the particle and can be used for acceleration.

As shown by Eq. (17), the wakefield for a point particle consists of an infinite set of modes (different k_m's). Real electron bunches have finite length and we can obtain the wakefield for them by integrating over the Green's function given by Eq. (17). (Actually the series in Eq. (17) does not converge and the expression only has physical meaning when used as a Green's function to integrate over a finite length current distribution.) For a beam with current distribution $I(ct-z)$ we find the synchronous wake is given by

$$E_z(r,\zeta) = \frac{k_0\epsilon^2}{c}\sum_{m=1}^{\infty} k_m \int_{-\infty}^{+\infty} d\zeta' I(\zeta')\cos[k_m(\zeta-\zeta')], \tag{18}$$

where $\zeta \equiv ct - z$. A particularly interesting current distribution is that of a linearly ramped beam with sharp cutoff, i.e., $I(\zeta) = I_0\zeta/L$ for $\zeta < L$, where L is chosen to be long compared with the longest mode (given by $p_m = p_1 \approx 2.4$). In this limit Eq. (18) gives

$$\begin{aligned} E_z &= \frac{I_0k_0\epsilon^2}{c}\sum_{m=1}^{\infty}\frac{1}{k_mL}\left(1-\cos k_m\zeta\right) \qquad \zeta < L \\ E_z &\approx \frac{I_0k_0\epsilon^2}{c}\sum_{m=1}^{\infty}\sin k_m(\zeta-L) \qquad \zeta > L. \end{aligned} \tag{19}$$

We note from Eq. (19) that the transformer ratio for each mode is $k_m L$. However, the higher order modes are not suppressed behind the beam as in other CWA concepts.[9] One can still obtain essentially a single mode wakefield by tailoring the end of the drive beam current to fall linearly over a distance $b << L$. In this case the field behind the beam becomes

$$E_z \approx \frac{I_0 k_0 \epsilon^2}{c} \sum_{m=1}^{\infty} \frac{1}{k_m b} \Big(\cos[k_m(\zeta - L - b)] - \cos[k_m(\zeta - L)] \Big). \tag{20}$$

For the modes with $k_m b << 1$ this expression reduces to that in Eq. (19), but the modes with $k_m b >> 1$ are suppressed.

For the case of a single mode, we find from Eqs. (19) or (20), that the amplitude of the accelerating wakefield is given by

$$E_z \approx \frac{I_0 k_0 \epsilon^2}{c} = 30 \frac{\mathrm{MV}}{\mathrm{m}} I_0(\mathrm{kA}) k_0(\mathrm{mm}^{-1}) \epsilon^2 \tag{21}$$

This amplitude is independent of the radial shape of the driving beam, but depends only on the peak current I_0. It increase linearly with k_0, which means shorter wavelength ripples in the waveguide wall produce larger wakefields. Furthermore, it depends only indirectly on the radius of the waveguide through the relative ripple amplitude ϵ. This parameter is the strongest leverage in obtaining a large field because of it's square dependence. Therefore, ϵ should be made as large as possible. Of course the analysis is only valid for $\epsilon << 1$ and increasing ϵ makes the waveguide more susceptible to breakdown.

Unfortunately, the amplitude of the fields indicated by Eq. (21) are somewhat modest by plasma wakefield standards for reasonably sized waveguides. However, in the limit $k_0 a >> 1$, we see from the definition of k_m below Eq. (17), that the lowest order modes become degenerate, i.e., $k_m \approx k_0/2$ for all m such that $(p_m/k_0 a)^2 << 1$. This means that instead of a single term in the sum in Eq. (20), we can get several. But because all the modes have the same wavelength this just multiples the amplitude of the wakefield given in Eq. (21) by the number of modes which are degenerate.

PARTICLE-IN-CELL SIMULATION METHOD

Numerical simulation of the wakefields and wakefield acceleration in rippled waveguides were performed using the particle-in-cell model ISIS. The algorithms were generalized to include a nonorthogonal coordinate system which had boundaries which conform the waveguide wall. The numerical algorithm is briefly described in this section. This algorithm is an improved version of an earlier body-fitted coordinate option in ISIS.[14]

The electric and magnetic fields are alternately advanced in time in a leap-frog fashion via Ampere's law and Faraday's law respectively. From the theory of relativity,[15] we know that Maxwell's equations can be written in the manifestly covariant form:

$$\partial \mathcal{F}^{\mu\nu}/\partial x^{\nu} = \mathcal{J}^{\mu} \tag{22}$$

and

$$\partial F_{\mu\nu}/\partial x^{\lambda} + \partial F_{\lambda\mu}/\partial x^{\nu} + \partial F_{\nu\lambda}/\partial x^{\mu} = 0, \tag{23}$$

where x^μ is the four-vector whose first 3 components are the coordinate components x^i ($i = 1,2,3$) and whose 4th component is $x^4 = ict$; t being the time and c is the speed of light. We have the following definitions:

$$\mathcal{F}^{\mu\nu} \equiv \begin{pmatrix} 0 & B_3 & -B_2 & -i\mathcal{E}^1 \\ -B_3 & 0 & B_1 & -i\mathcal{E}^2 \\ B_2 & -B_1 & 0 & -i\mathcal{E}^3 \\ i\mathcal{E}^1 & i\mathcal{E}^2 & i\mathcal{E}^3 & 0 \end{pmatrix} \text{ and } \mathcal{J}^\mu \equiv \begin{pmatrix} \mathcal{J}^1 \\ \mathcal{J}^2 \\ \mathcal{J}^3 \\ ic\varrho \end{pmatrix} \tag{24}$$

where $\mathcal{E}^i$ and $\mathcal{J}^i$ are the contravarient vector density components of the electric field and current density respectively and B_i is the covariant component of the magnetic field. $\varrho \equiv \sqrt{g}\tilde{\rho}$, where $\tilde{\rho}$ is the physical charge density. Note that the (appropriately weighted) sum of the charges on the particles in a cell gives ϱ for that cell and not $\tilde{\rho}$. The metric tensor $g_{\mu\nu} \equiv \partial\vec{r}/\partial x^\mu \cdot \partial\vec{r}/\partial x^\nu$ where $\vec{r}$ is a four-vector with the usual first three spatial components and ict as an orthogonal fourth component. The quantity $g^{\mu\nu}$ is defined by $g^{\mu\nu}g_{\mu\nu} = 1$ and $\sqrt{g} = \sqrt{\det(g_{\mu\nu})}$. The quantity $F_{\mu\nu}$ is given by

$$F_{\mu\nu} = \frac{1}{\sqrt{g}} g_{\mu\lambda}g_{\nu\sigma}\mathcal{F}^{\lambda\sigma} \tag{25}$$

This tensor can be a complicated function of the physical field components, depending on the complexity of the metric tensor. For generalized cylinarical coordinates $x^1(z,r)$ and $x^2(z,r)$, where z and r are the usual cylindrical coordinates, and the ignorable coordinate $x^3 = \theta$, the metric tensor becomes

$$g_{\mu\nu} = \begin{pmatrix} {z_1}^2 + {r_1}^2 & z_1z_2 + r_1r_2 & 0 & 0 \\ z_1z_2 + r_1r_2 & {z_2}^2 + {r_2}^2 & 0 & 0 \\ 0 & 0 & r^2 & 0 \\ 0 & 0 & 0 & 1 \end{pmatrix}, \tag{26}$$

where the subscripts 1 and 2 denote differentiation with respect to x^1 and x^2, respectively. If the mesh and hence the metric are not functions of time then $F_{\mu\nu}$ takes the following simple form

$$F_{\mu\nu} = \begin{pmatrix} 0 & \mathcal{B}^3 & -\mathcal{B}^2 & -iE_1 \\ -\mathcal{B}^3 & 0 & \mathcal{B}^1 & -iE_2 \\ \mathcal{B}^2 & -\mathcal{B}^1 & 0 & -iE_3 \\ iE_1 & iE_2 & iE_3 & 0 \end{pmatrix}, \tag{27}$$

where E_i are the covariant components of the electric field and $\mathcal{B}^i$ are the contravarient vector density components of the magnetic field. In ISIS the $\mathcal{E}^i$'s and $\mathcal{B}^i$'s are saved in arrays and the covariant components are constructed as needed from $E_i = g_{ij}\mathcal{E}^j/\sqrt{g}$ and $B_i = g_{ij}\mathcal{B}^j/\sqrt{g}$ (the sum over j is from 1 to 3). The metric elements are obtained from arrays of values of r and z on the logical grid using finite differencing of Eq. (26).

The spatial differencing is performed according to a staggered grid which for orthogonal coordinates reduces to the differencing devised by Godfrey.[16] The boundary condition for the fields are that the tangential electric field vanish on a conductor. This is equivalent

to the requirement that the covariant component not normal to the surface vanish. For nonorthogonal coordinate systems ($g_{12} \neq 0$) this involves averaging to obtain E_i and B_i. Poisson's equation is not used, but the differencing insures that it is satisfied for all time if it is satisfied initially,[17] provided the accumulated current satisfies the continuity equation

$$\partial \mathcal{J}^\mu / \partial x^\mu = 0. \tag{28}$$

The prescription used to do this is the same as used by Morse and Nielson[18] in Cartesian coordinates, where we note that the quantity actually obtained is $\mathcal{J}^i$. ISIS also uses a pyramid shaped particle to ameliorate the high frequency noise associated with this method[19]. The particle pusher used is the Boris algorithm.[20] Because the velocities are not needed to obtain the current densities, the particle momenta used are the orthogonal $r-z$ values. In a fashion similar to that used for the field equations the metric elements are interpolated for each particle from the values of z and r on the grid. The field quantities are known at time-step $n + 1/2$. First the contravarient components of the fields are linearly weighted for each particle. Then the fields are converted to cylindrical orthogonal coordinates by

$$E_z = (z_1 \mathcal{E}^1 + z_2 \mathcal{E}^2)/\sqrt{g} \tag{29}$$

$$E_r = (r_1 \mathcal{E}^1 + r_2 \mathcal{E}^2)/\sqrt{g} \tag{30}$$

$$E_\theta = \mathcal{E}^3 r/\sqrt{g} \tag{31}$$

and similar equations for the magnetic field components.

The position update proceeds by converting to a local cylindrical coordinate system. The values of x^1 and x^2 are used to interpolate to values of z and r for the particle. The change in the cylindrical coordinate positions Δz and Δr are found by the usual prescription of converting to a local Cartesian coordinate system. The particles new position on the $x^1 - x^2$ grid is found from the approximate relations

$$x^{1(n+1/2)} = x^{1(n-1/2)} - \frac{z_2 \Delta r}{J} + \frac{r_2 \Delta z}{J} \tag{32}$$

$$x^{2(n+1/2)} = x^{2(n-1/2)} + \frac{z_1 \Delta r}{J} - \frac{r_1 \Delta z}{J}, \tag{33}$$

where $J \equiv z_1 r_2 - z_2 r_1$. This procedure is iterated twice to insure accuracy.

PARTICLE-IN-CELL SIMULATION RESULTS

Simulations of wakefield generation and subsequent acceleration were performed using the particle-in-cell algorithm described in the last section. As shown in Eq. (21), large accelerating gradients are obtained by choosing large k_0. Furthermore as discussed in that section an amplification of the wakefield due to degeneracy of the lowest order modes is obtained in the limit $k_0 a >> 1$. Two simulations performed under these conditions will be discussed in this section.

The simulation results scale with the drift tube radius, a. The total length of the simulation is $80a$. The parameters of the simulations are as follows: $k_0 a = 10$; the drive

beam current in linearly ramped from 0 to a peak value of $I_0 = 20$ kA in a distance $L = 6.0a$; the current then falls quickly in a distance of $b = 0.2a$; the factional ripple depth is $\epsilon = 0.2$. The number of cells in the axial (z) direction is 2000 and the number of cells in the radial (r) direction is 25. The time-step is $\delta t = 0.02a/c$.

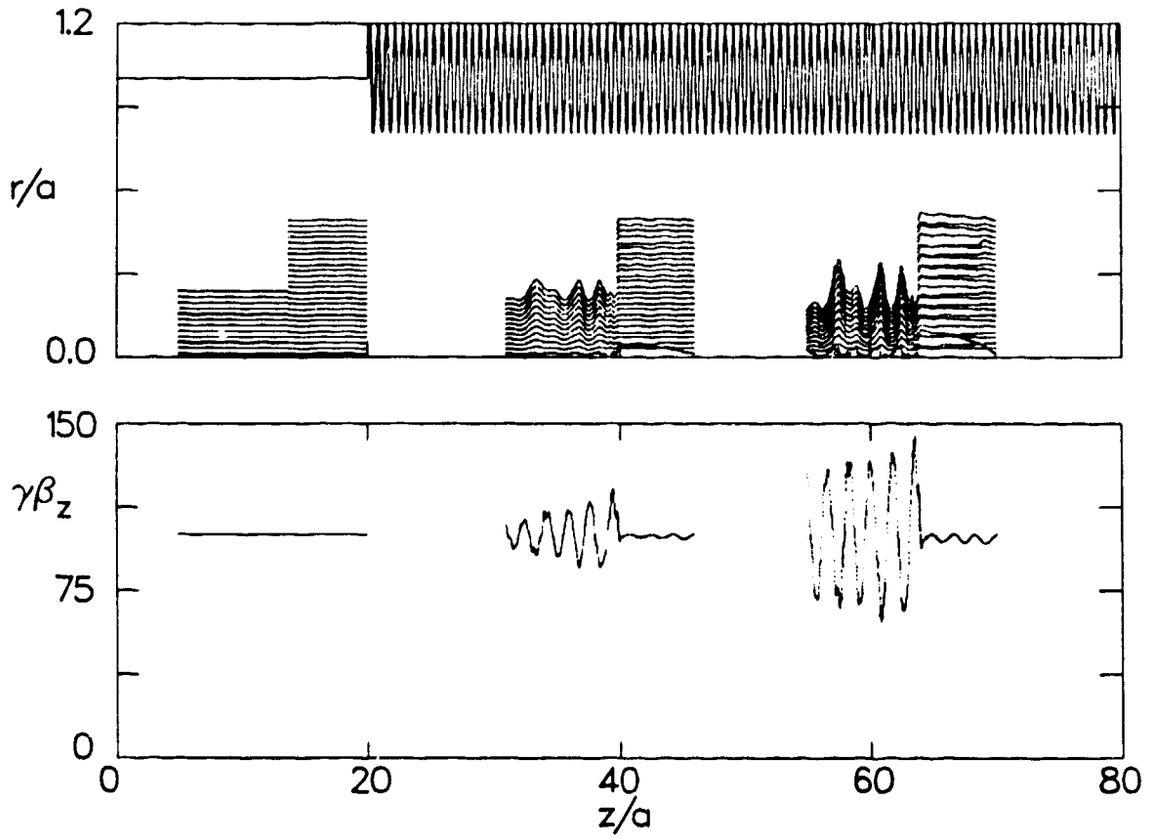

Fig. 1 Results of self-consistent particle-in-cell simulation. The upper plot shows the geometry and snapshots of the beams at three different times. The lower plot is the momentum of the beams versus axial postion, showing deceleration of the drive beam and acceleration of the trailing beam.

In the first simulation shown in Fig. 1, both the drive beam and trailing witness beam have initial energies of 50 MeV. The upper plot in Fig. 1 shows the geometry and snapshots of the particle positions at three different times. The bottom plot shows the longitudinal phase space at the same three times. The drive beam's radius is initially $0.5a$ and the witness beam's radius is initially $0.25a$. The simulations are initialized by injecting the beams from the left in the region where the drift tube wall is straight and equal to a. The particles are given an artificially large mass so they do not respond to the field produced as they are injected. This procedure, eliminates transients associated with injection through the left boundary and allows the self-consistent calculation of the fields for the proper beam velocity. At the instant of the first snapshot the particles are given the correct electron mass and allowed to evolve self-consistently as they enter the region

of the rippled guide. The trailing beam has vanishingly small charge and serves only to sample the wakefields generated by the driving beam.

The effects of the wakefield acceleration can be seen in the phase space plot in Fig. 1. For the parameters chosen the first four modes have wavelengths of $\lambda_1 = 1.19a, \lambda_2 = 0.96a, \lambda_3 = 0.72a, \lambda_4 = 0.53$. Considering the fall time, we would expect the first 2 or 3 modes to be excited, so that the synchronous wakefield amplitude from Eq. (21) should be 50-70 MV/m for $a = 1$ cm. Of course, reducing a by a factor of 2 increases the wakefield by a factor of 2. The estimate of the wakefield obtained in the simulation from the acceleration of the trailing beam is 50 MV/m for $a = 1$ cm, in good agreement with the analysis. Furthermore, as can be seen in the phase space plot, the wakefield is nearly a single mode with wavelength, $\lambda \approx a$, also as predicted. Furthermore, the transformer ratio as seen by comparing the maximum deceleration in the drive beam with the maximum acceleration of the drive beam is about 5-6 as predicted.

As mentioned earlier, the synchronous transverse wake vanishes (to order $1/\gamma^2$). This is easily seen from the Fourier transform of Faraday's law.

$$E_r = \frac{kc}{\omega} B_\theta \tag{34}$$

When the phase velocity of the wave (ω/k) is the speed of light, c, $E_r = B_\theta$ and the transverse force on an ultrarelativistic particle vanishes. However, there are as mentioned earlier, nonsychronous wakefields generated. From Eq. (12), we see that they are first order in ϵ. For modes, such that $k_0 a >> p_n$ we find that the phase velocity of the waves is approximately $-c$. These waves move quickly backward through the beams and provide no net energy loss or gain to the beams. However, even though these modes are not synchronous, they can have an effect on wakefield accelerators. Firstly, from Eq. (34), there can be a instantaneous net radial force on the beams because $\omega/k \neq c$. The effect is to wiggle the beam particles up and down with no net energy gain. Though this effect may not drive the beams into the wall, it may increase the transverse emittance and cause synchrotron radiation at higher energies. This transverse motion, is seen in the snapshots of the particle positions in Fig. 1. The effect is almost unmeasurable for the driving beam, but noticeable for the trailing beam. Secondly, because the nonsynchronous wakefield is first order in ϵ, it will be roughly a factor of $1/\epsilon$ larger than the accelerating field. Thus this field may become a limiting factor in the accelerating gradient obtainable because the waveguide wall may breakdown from this field

There appears to be a filamentation instability beginning to be seen in the drive beam in the upper plot in Fig. 1. Though it has not been analyzed, this instability is probably analogous to the Weibel instability observed in plasma wakefield studies,[5,6] with the slow wave structure of the rippled guide serving the function of the plasma. Other simulations show this instability to be a function of the drive beam energy and current. Figure 2 shows the results of a simulation identical to the one in Fig. 1 except the drive beam has an initial energy of 20 MeV. The filamentation of the drive beam is significantly worse in this case. However, as shown in the analysis, the wakefield is independent of the radial profile of the drive beam. Thus as shown in Fig. 2, the acceleration and transverse effects on the trailing beam by the filamentation of the drive beam are unmeasurable. This

is rather different than the case of the plasma wakefield accelerator, where filamentation of the drive beam imposed strong filamentation in the trailing beam.[5]

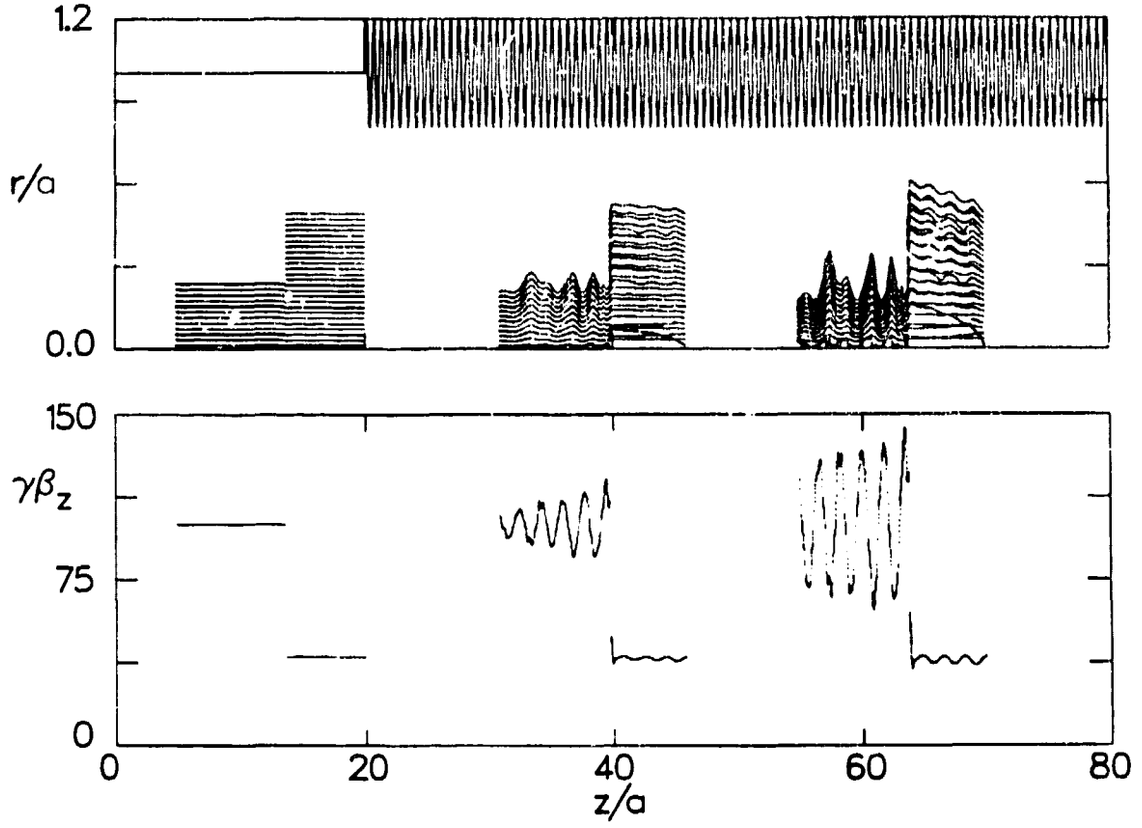

Fig. 2 Simulation results for same parameters as in Fig. 1, except for 20 MeV driving beam energy instead of 50 MeV. Filamentation of the drive beam is more pronounced, but the trailing beam is unaffected by the filamentation.

SUMMARY AND CONCLUSIONS

Analysis and simulation of wakefield generation and acceleration indicate that interesting accelerating gradients may be obtained. The accelerating field is found to depend linearly on the peak drive beam current for linearly ramped beams and quadratically on the fractional ripple depth, ϵ. Improvements in the accelerating field can be obtained by increasing the ripple wavenumber, k_0. This is stronger than linear dependence, because the amplitude for a single mode scales as k_0 as shown in Eq. (21) and more modes will be degenerate. The field is independent of the radial distribution of the drive current, and though the system may be subject to a filamentation instability for sufficiently long drive beams, this property makes the accelerating field insensitive to the filamentation effect.

ACKNOWLEDGMENTS

The authors would like to acknowledge useful discussions with R. K. Cooper and R. L. Gluckstern.

REFERENCES

1. G. A. Voss and T. Weiland, DESY M82-10 (1982).
2. R. Ruth, A. W. Chao, P. L. Morton, and P. B. Wilson, Part. Accel. **17**, 171 (1985).
3. P. Chen, J. M. Dawson, R. W. Huff, and T. Katsouleas, Phys. Rev. Lett. **54**, 693 (1985).
4. R. K. Keinigs, M. E. Jones and W. Peter, "A Comparison of the Dielectric and Plasma Wakefield Accelerators," submitted to Phys. Fluids.
5. R. K. Keinigs and M. E. Jones, Phys. Fluids. **30**, 252 (1987).
6. J. J. Su, T. Katsouleas, J. M. Dawson, P. Chen, M. E. Jones and R. K. Keinigs, IEEE Trans. on Plasma Sci. **PS-13**, 192 (1987).
7. C. Callan, D. Hammer, C. Max, F. Perkins, and M. Rosenbluth, " A Ferrite-Loaded Gapless Wakefield Accelerator," JASON Report JSR-86-109 (March 1987).
8. A. Ruggiero, P. Schoessow, and J. Simpson, in *Advanced Accelerator Concepts*, edited by F. Mill, AIP Conference Proceedings No. 156 (American Institute of Physics, New York, 1987), p. 247
9. R. K. Keinigs, M. E. Jones and W. Gai, "The Cherenkov Wakefield Accelerator," to be published in Part. Accel..
10. W. Gai, P. Schoessow, B. Cole, R. Konecny, J. Norem, J. Rosenzweig, and J. Simpson, Phys. Rev. Lett. **61**, 2756 (1988).
11. M. Chatard-Moulin and A. Papiernik, IEEE Trans. Nucl. Sci. **26**, 3523 (1979).
12. R. K. Cooper, S. Krinsky, and P. L. Morton, Part. Accel. **12**, 1 (1982).
13. R. L. Gluckstern, "Longitudinal Impedance of a Periodic Structure at High Frequency," to be published in Phys. Rev. D.
14. M. E. Jones, "Electromagnetic PIC Codes with Body-Fitted Coordinates," *Proceedings of the 12th Conf. on Num. Sim. of Plasmas*, San Francisco, Ca., Sep. 20-23, 1987, LA-UR-87-2522.
15. W. Pauli, *Theory of Relativity*, (Dover Pub., New York, 1981), pp. 156-157.
16. B. B. Godfrey, "Application of Galerkin's Method to Particle- in-Cell Plasma Simulation," LA-UR-78-1311, *Proc. Eighth Conf. Num. Sim. Plasmas*, Monterey, Ca., Jun. 28-30, 1978.
17. G. R. Gisler and M. E. Jones, "Charge-Conserving Algorithms Versus Poisson Corrections for Electromagnetic PIC Codes," *Proc. Eleventh Conf. Num. Sim. Plasmas*, Montreal, Jun. 25-27, 1985.
18. R. L. Morse and C. W. Nielson, Phys. Fluids **14**, 830 (1971).
19. A. Bruce Langdon, Phys. Fluids **15**, 1149 (1972).
20. J. P. Boris, it Proc. Fourth Conf. Num. Sim. Plasmas, Naval Res. Lab., Washington, D.C., p. 3, Nov. 2-3, 1970. and A. B. Langdon and B. F. Lasinski, "Electromagnetic and Relativistic Plasma Simulation Models," *Meth. Comput. Phys.* **16**, p. 327, B. Alder, S. Fernbach, M. Rotenberg, and J. Killeen, eds. (Academic, New York, 1976).